Check for updates

Science RESEARCH ARTICLE FIRST RELEASE

QUANTUM GASES

Quantum gases below 10 picokelvin in space

Wei Xiong[1]†, Tang Li[2]†, Shengjie Jin[3]†, Qi Huang[1,3], Bin Wang[2], Lin Li[2], Yufeng He[4], Xiaopeng Li[5], Dijun Chen[2], Tieqiang Song[2], Jingwei Ji[2], Cuiyun Zhou[2], Chi-Kin Lai[1], Zhengxi Zhang[1], Jinyuan Tian[1], Yajing Guo[3], Hepeng Yao[1], Xia Hou[2], Liang Liu[2], Xiaoji Zhou[1]*, Weibiao Chen[2]*, Xuzong Chen[1]*

Ultracold atom platforms enable low temperatures and long free evolution times, which are crucial for fundamental physics tests and atom interferometry. The lowest equivalent temperature reported in such a system is 38 pK with a free expansion time of 2 s, achieved in atom-chip-based magnetic traps in microgravity. Optical dipole trap (ODT) systems offer better optical access and the flexibility to condense both magnetic and non-magnetic atoms, but have not been used to prepare quantum degenerate gases under microgravity conditions. Here we report an ODT-based Bose-Einstein condensate created aboard the China Space Station, containing 2.0×10^4 atoms, reaching an equivalent temperature of $9.7^{+3.2}_{-2.7}$ pK with a free expansion time of 7.0 s. This record-low temperature could stimulate a new generation of ODT-based experiments in quantum simulation and precision measurements in space.

Lowering the temperature of atomic gases has long been an important goal. Evaporative cooling opened access to the nanokelvin regime, enabling the creation of quantum gases such as Bose-Einstein condensates (BECs) (*1*, *2*) and degenerate Fermi gases (*3*). These ultracold systems serve as versatile platforms for quantum simulation (*4*–*6*), precision measurement (*7*–*9*), and fundamental studies of phase transitions (*10*). Further cooling into the picokelvin range enabled the realization of exotic quantum states, such as Bose glass and fractal Mott insulators (*11*, *12*), and ultra-sensitive experiments including tests of the equivalence principle (*13*, *14*), gravitational wave detection (*15*, *16*), and dark energy searches (*17*). In terrestrial experiments, deep cooling methods can reach 350 pK in three dimensions (*18*, *19*), and 50 pK in two dimensions (*20*). Earth's gravity, however, poses a challenge for further advances (*21*). To counteract the effects of gravitational sag and retain atoms, there is always a finite confining trap frequency during evaporative cooling, which consequently limits the achievable temperature (*22*). Although magnetic levitation can compensate for gravity (*18*), it introduces residual curvature that restricts further reduction of the trap frequency (*23*).

Microgravity platforms, including drop towers (*24*–*26*), Einstein elevators (*27*), zero-g aircraft (*28*–*30*) and sounding rockets (*31*), offer a powerful means to temporarily mitigate gravitational constraints and push ultracold atomic systems toward lower energy scales. This energy scale can be quantified by the equivalent temperature (*26*, *32*), which represents the average kinetic energy of a quantum gas during free expansion. For instance, the previously reported lowest equivalent temperature is 38 pK in drop towers (*26*). Limited by the free fall time of the experiment, the free evolution of the atomic ensemble could be followed up only to 2 s (*26*). A long expansion time of quantum gases significantly benefits quantum sensing, as the sensitivity of atomic interferometers typically scales with the square of this free expansion time (*21*); this enhanced capability may contribute to cutting-edge experiments (*13*–*17*, *33*). However, the microgravity durations on these platforms are inherently limited by the continuous operation periods achievable under microgravity conditions. To further explore the potential of quantum gases at picokelvin temperatures, long-duration orbital platforms have been developed. The only previously reported in-orbit platform to date is the Cold Atom Laboratory (CAL), an atom-chip-based magnetic system aboard the International Space Station (*32*–*37*). CAL experiments have produced ultracold atomic gases with equivalent temperatures reaching 52 pK using matter-wave lensing techniques (*32*), along with free expansion times of up to 1 s (*34*).

Whereas atom-chip-based magnetic traps have achieved ultralow temperatures, their optical dipole trap (ODT) counterparts have yet to reach comparable performance. Compared to magnetic traps, ODTs can accommodate tunable interactions and optical potentials of various configurations, including optical lattices. They also grant direct access to spinor quantum gases (*38*), in which the spin degrees of freedom are not frozen by an external magnetic field. Coherent manipulation of such spinor systems enriches the possibilities for quantum simulation and atomic interferometry. Several ground-based microgravity platforms have explored ODT protocols: evaporative cooling to microkelvin temperatures has been achieved in drop towers (*39*), and BEC expansion dynamics studied in Einstein elevators (*27*). However, owing to the limited duration of microgravity on these platforms, the use of ODTs to directly prepare quantum degenerate gases under microgravity conditions has not been demonstrated.

Here we report an optical-dipole-trap realization of BECs in space, with an equivalent temperature below 10 pK. This breakthrough is enabled by a two-stage cooling protocol in ODTs (*21*, *40*–*42*) implemented with a stable, high-power crossed-beam ODT system aboard the China Space Station, *Tiangong*. The final three-dimensional equivalent temperature is $T_{\mathrm{eq}} = 9.7^{+3.2}_{-2.7}$ pK, which is, to our knowledge, the lowest equivalent temperature ever measured. Notably, the ultracold atomic cloud remains visible even after 7.0 s of free expansion. Our platform opens up new avenues for exploring physics at these extremely low temperatures, and may enable next-generation atom interferometers (*25*, *33*, *37*, *43*–*46*) that exploit intrinsic spin dynamics and long-duration expansion.

Tiangong Cold Atom System in space

The Cold Atom Physics Rack (CAPR, Fig. 1A), housed in the *Mengtian* experimental module aboard the China Space Station *Tiangong* (Fig. 1B), has been operating nominally since its successful launch on 31 October 2022. As described in Refs. (*47*, *48*), CAPR integrates a physical package, laser systems for cooling, optical trapping and lattices, as well as an electronic control module, see details in Fig. 1A. All components are interconnected via optical fibers and electrical cabling, enabling modular integration and future subsystem upgrades. Atomic cooling operations are primarily carried out within the physical package. Atoms are pre-cooled in a two-dimensional vacuum chamber before being transferred to the Science Chamber, where laser and evaporative cooling are performed (Fig. 1C). Figure 1, D and E, show the key components of the Science Chamber: pairs of magnetic coils generating

[1]School of Electronics, Peking University, Beijing, China. [2]Aerospace Laser Technology and System Department, Shanghai Institute of Optics and Fine Mechanics, Chinese Academy of Sciences, Shanghai, China. [3]International Center for Quantum Materials, School of Physics, Peking University, Beijing, China. [4]Technology and Engineering Center for Space Utilization, Chinese Academy of Sciences, Beijing, China. [5]Department of Physics, Fudan University, Shanghai, China. ***Corresponding author. Email: xjzhou@pku.edu.cn (X.Z.); wbchen@siom.ac.cn (W.C.); xuzongchen@pku.edu.cn (X.C.)** †These authors contributed equally to this work.

Downloaded from https://www.science.org at Peking University on November 05, 2026

bias fields, gradients and magnetic traps, six laser cooling beams, orthogonal imaging systems along the y- and z-axes (Probing-H and Probing-V), and two crossed ODTs configurations. Each ODT is formed by two laser beams intersecting at 60°, with their bisectors aligned along the x- and y-axes (Fig. 1E). The dual-ODT configuration comprises ODT1, with a tighter waist (54 m) for evaporative cooling, and ODT2, with a larger waist (124 m) used for quasi-adiabatic expansion. The opto-mechanical system maintains micron-level structural stability before and after the payload launch through integration of laser sources and reconfigurable control optics (*49*).

BEC Formation in a Space ODT

We begin with evaporative cooling process for preparing BECs, which is the first stage of cooling in the ODTs. Following laser cooling procedures similar to those used in terrestrial experiments (*48*), we load approximately 2.0×10^6 ^{87}Rb atoms in the $|F = 1\rangle$ hyperfine manifold into ODT1 for evaporative cooling (*49*). At the start of evaporation, each beam of ODT1 operates at a power of 5.0 W, which is gradually reduced throughout the cooling process. Figure 2A displays absorption images taken as P_{ODT1} (the power at which ODT1 is turned off) decreases from 13.0 mW to 1.0 mW during the final stage of evaporation. As the trap depth is lowered, the atomic cloud becomes more condensed and its central optical density (OD) increases. Meanwhile, the temperature drops from 112 nK to 6 nK, and the phase-space density (PSD) rises sharply, signaling the onset of BEC. Notably, atoms remain not only near the center but also in the wings of ODT1, potentially affecting the bimodal fit of the momentum distribution; this influence is mitigated by our analysis (*49*).

Because the atomic spins remain unpolarized throughout the evaporation process, the resulting condensate is a spinor BEC. To probe the spin composition, we apply a Stern–Gerlach sequence (*50*), to spatially separate the $|F = 1, m_F = +1, 0, -1\rangle$ Zeeman components by imposing a magnetic field gradient of 1.3 G/cm for the first 15 ms of a 20 ms TOF. Figure 2B displays the spatial distributions of these three spin states throughout evaporation. As P_{ODT1} falls below 8.0 mW, three distinct peaks emerge, corresponding to the three spin components. A typical image at $P_{\mathrm{ODT1}} = 1.0$ mW is shown in the inset of Fig. 2B. We fit the density profile along the z-axis (blue circles) with a triple bimodal distributions (red lines), each representing a spin component (*49*). In all three cases, the fitted results exhibit clear bimodal distributions, demonstrating the formation of a spinor BEC. The asymmetric peak heights in Fig. 2B may originate from a residual magnetic field.

The condensate fraction of this spinor BEC reaches a maximum of 65% when P_{ODT1} is reduced to 0.2 mW (Fig. 2C, green circles). This corresponds to trap frequencies of $(\omega_x, \omega_y, \omega_z) = 2\pi \times (3.3, 5.7, 6.6)$ Hz, with a total atom number of 2.7×10^4 and a temperature of 4.8 nK. This maximum condensate fraction in space is still notably lower than the highest values typically achieved in ground-based experiments. To study this difference, we further compare the evolution of the condensate fraction during evaporative cooling in ground-based CAPR-analogous systems (purple circles in Fig. 2C) and in space (green circles), which shows the differences between the two environments. First, the P_{ODT1} threshold for BEC formation in space is approximately 8.0 mW, which is significantly lower than ground-based experiments (45.0 mW). Second, the ground-based system reaches a condensate fraction of 89% at a final power of 20.0 mW within 5 s (purple circles in Fig. 2C), whereas the space-based counterpart requires ~20 s to achieve a lower condensate fraction of 65% at a final power of 0.2 mW (green circles in Fig. 2C). In addition, atoms are visibly distributed in the wings of the ODT1 in space—a feature absent in ground-based observations (Fig. 2C, right insets). These observations underscore the differences in ODT-based evaporative cooling between ground and microgravity environments. On Earth, gravitational sag tilts the trapping potential, facilitating the removal of high-energy atoms and enhancing evaporation efficiency-thereby enabling higher condensate fractions. By contrast, in microgravity, the absence of such gravitational tilting reduces evaporation efficiency. Achieving higher condensate fractions in space thus requires further reduction of the trap depth, which is limited by slower thermalization rates and greater susceptibility to external noise under ultrashallow confinement.

To further increase the condensate fraction at this stage within the permissible experimental conditions in space, we introduce a magnetic field gradient during the evaporative cooling process in ODT1. The field gradient mimics gravity-like forces to enhance evaporation efficiency (*51*), but it selectively acts on magnetically-sensitive $|1, \pm1\rangle$ states. This scheme aims to achieve similar process to sympathetic cooling (*52*, *53*) and enhances the cooling efficiency of $|1, 0\rangle$ by accelerating $|1, \pm1\rangle$ evaporation and leveraging $|1, \pm1\rangle$-$|1, 0\rangle$ collisions (*49*). In the experiment, we apply a magnetic field gradient of $\nabla B = 4.1$ G/cm to lower the trap depth experienced by the $|1, \pm1\rangle$ states atoms, along with a bias field to preserve the atomic magnetic moments. The blue circles in Fig. 2C show the evolution of condensate fraction under this protocol, where the BEC formation threshold shifts from 8.0 mW to 20.0 mW, indicating accelerated evaporation process with the nonzero magnetic field gradient applied. The population fraction of atoms in the $|1, 0\rangle$ state during the evaporation process is shown in Fig. 2C, left inset. When P_{ODT1} decreases to 20.0 mW, the $|1, 0\rangle$ population is approximately 40%. As P_{ODT1} drops further to 10.0 mW, this fraction rapidly rises to over 80%. Upon further evaporation down to 0.2 mW, the $|1, 0\rangle$ fraction slowly approaches nearly 100%. These results reveal a dramatic redistribution of atomic populations among different Zeeman sublevels in the final stages of evaporation. We attribute this to two main factors: first, as P_{ODT1} decreases to lower values, the magnetic field gradient exerts a stronger influence on the trapping potential, causing significant losses of atoms in the $|1, \pm1\rangle$ states (*49*); second, the quadratic Zeeman effect causes energy shifts that favor the spin-changing collisional transfer of atoms from $|1, \pm1\rangle$ to $|1, 0\rangle$, making the reverse process less likely (*54*). Finally, at 0.2 mW, we obtain a nearly pure $|1, 0\rangle$ BEC containing 2.3×10^4 atoms, with a condensate fraction of 89% at a thermodynamic temperature of 3.1 nK—over 20% higher than without the magnetic gradient.

Up to this stage, we have discussed the thermodynamic temperature determined by the bimodal fit of the momentum distribution (*18*). However, after achieving the BEC, the equivalent temperature T_{eq}, which usually characterizes the expansion energy and determines the expansion velocity of the quantum gases, is a more relevant parameter than the thermodynamic temperature, see Refs. (*20*, *25*, *26*, *32*, *34*). For applications like atomic interferometry, T_{eq} limits the duration of the interferometer and the sensitivity, thus serving as a key indicator for evaluating its performance (*25*, *26*, *32*, *34*). Hence, after the first-stage cooling, we focus on strategies to further lower T_{eq} or the expansion energy. This energy mainly originates from the interaction energy E_{int} that is released when the trap is turned off, following $3k_B T_{\mathrm{eq}} / 2 = E_{\mathrm{int}} / N$ with N the atom number and k_B the Boltzmann constant. To explore the reduction of T_{eq} in the CAPR, we first derive its dependence at equilibrium on the relevant parameters in a crossed ODT configuration (*49*) and find

$$T_{\mathrm{eq}} \propto N^{2/5} P^{3/5} w^{-12/5} \tag{1}$$

with N the atom number, w the beam waist radius, and P the laser power. According to Eq. 1, T_{eq} scales strongly with the beam waist as $T_{\mathrm{eq}} \propto w^{-12/5}$, indicating that increasing the waist radius can dramatically reduce the expansion energy. Equation 1 thus predicts that transferring

Downloaded from https://www.science.org at Peking University on November 05, 2026

the atoms from ODT1 into ODT2, which has a significantly larger beam waist $w_2 = 124$ m, would reduce the equivalent temperature in ODT2 by a factor of 7.4 compared to ODT1 at the same light power and atom number.

Cooling Quantum Gases below 10 pK

In the actual experiment, we further cool the quantum gases by a second-stage cooling protocol proposed in Ref. (*21*, *40*–*42*). Different from the previous delta-kick cooling method in magnetic traps (*20*, *25*, *26*, *32*), this protocol is a purely optical protocol that benefits from the mechanism of Eq. 1. The main step is to transfer atoms from ODT1 into ODT2 and ramp down the power of ODT2 to 12.5 W, corresponding to trap frequencies $(\omega_x, \omega_y, \omega_z) = 2\pi \times (0.17, 0.29, 0.33)$ Hz, within a decompression time. According to the requirements of Eq. 1, a strictly adiabatic decompression would be needed to maintain thermal equilibrium. However, because the power of ODT2 is on the order of tens of microwatts, achieving such an adiabatic process would require several hundreds seconds, which would be severely affected by environmental noise. Therefore, we instead implement a non-adiabatic (quasi-adiabatic) decompression (similar to Refs. (*20*, *26*, *32*, *34*)), with a decompression duration of 1.175 s (*49*).

Subsequently, after switching off ODT2, we allow the atomic cloud to expand freely for various TOFs, followed by absorption imaging using both the Probing-H and Probing-V systems. The Probing-V results, shown in Fig. 3A, illustrate the evolution of atomic density profiles in the *xy*-plane versus TOF; the *z*-direction distribution can be obtained from the Probing-H results. During free expansion, variations in the atomic cloud size reflect its expansion energy, which can be used to evaluate T_{eq}. This method of evaluating T_{eq} is a commonly adopted approach in previous studies (*26*, *32*, *34*). By fitting these distributions, we extract the Thomas–Fermi radii $R_{\mathrm{TF}-i}$ $(i = x, y, z)$ of the atomic gas in the x, y, and z directions, which characterize the cloud size along each spatial axis, as plotted in Fig. 3B (*49*). During free expansion, the interaction energy of the atoms is converted into kinetic energy. For TOFs exceeding 300 ms, the cloud size increases to more than $e^{1/3} \approx 1.4$ times its initial value, reducing both density and interaction energy to approximately $1/e$ of their original values, effectively rendering interactions negligible. In this regime, the expansion is dominated by the atoms' kinetic energy. Therefore, we use data with TOF >300 ms to perform linear fits to the cloud sizes (Fig. 3A) (*32*), yielding expansion velocities of $V_x = 70^{+12}_{-12}$ m/s, $V_y = 88^{+12}_{-12}$ m/s, and $V_z = 83^{+13}_{-13}$ m/s, corresponding to an equivalent temperature of $T_{\mathrm{eq}}^{(\mathrm{exp})} = 9.7^{+3.2}_{-2.7}$ pK.

T_{eq} is sensitive to the decompression time and reaches its minimum at 1.175 s (Fig. 3B, inset). For shorter decompression times, T_{eq} rises rapidly owing to increased excitations from overly rapid decompression. When the decompression time exceeds this optimum, T_{eq} slightly increases, reflecting the cumulative effects of noise and system fluctuations. We therefore adopt 1.175 s as an optimal trade-off between cooling performance and experimental stability. We also compare the experimentally obtained equivalent temperature, $T_{\mathrm{eq}}^{(\mathrm{exp})}$, with numerical simulations under identical experimental parameters, which yield $T_{\mathrm{eq}}^{(\mathrm{sim})} = 7.4$ pK (*49*). These two results show reasonable agreement. The discrepancy between $T_{\mathrm{eq}}^{(\mathrm{exp})}$ and $T_{\mathrm{eq}}^{(\mathrm{sim})}$ is likely caused by experimental imperfections such as excitation and heating introduced by fluctuations in pointing and intensity of ODT2.

Figure 3C presents single-shot absorption images of the atomic cloud at extended TOFs ranging from 2.0 s to 7.0 s. Notably, atoms remain visible even at 7.0 s owing to the dramatic suppression of expansion energy and the attainment of an ultralow equivalent temperature. This capability lays a crucial foundation for future high-precision atomic interferometry in space-based platforms. Because the signal-to-noise ratio of images with TOF exceeding 2.0 s is relatively low, we use images within 2.0 s of TOF to evaluate the equivalent temperature.

Discussion and outlook

In conclusion, we have established a space-based ultracold bosonic gas laboratory aboard the China Space Station, and successfully generate a BEC under ten picokelvin scale. This all-optical platform enables a two-stage cooling protocol in ODTs. In the first stage of cooling in a crossed optical dipole trap, we obtain a spinor BEC, and further achieve a degenerate gas in a Zeeman state of $m_F = 0$ with a high condensate fraction by applying evaporative cooling together with a magnetic field gradient. This magnetically insensitive condensates serve as ideal initial states for atomic interferometers, providing enhanced immunity to magnetic field fluctuations. By transferring the atoms to a second, wider optical dipole trap and releasing them quasi-adiabatically, we significantly reduce the expansion energy, reaching an equivalent temperature of $T_{\mathrm{eq}} = 9.7^{+3.2}_{-2.7}$ pK. The atomic ensemble remains spatially resolvable even following the TOF expansion of 7.0 s. In future experiments, the atom number could be increased by employing a tunable-volume optical trap, such as the apparatus described in Ref. (*55*). Our results prove the ODT-based platform in orbit is a powerful tool for generating quantum gases at ultralow temperature. This all-optical ultracold platform, readily compatible with versatile control schemes such as three-dimensional optical lattices, meets the exacting requirements for quantum simulation and precision metrology in future space missions, thus positioning it to advance two primary scientific frontiers. First, it aims to enable quantum simulation for exploring low-temperature physics in the unique environment of space. This includes the study of exotic quantum phases, such as investigating the decay of Tomonaga-Luttinger liquid order in one-dimensional bosonic systems (*56*–*58*) and probing the properties of Bose-glass or fractal Mott phases in disordered potentials (*11*, *12*). A second possible objective is the construction of a space-based atom Mach-Zehnder interferometer (*25*, *33*, *37*, *43*–*46*), with the potential to perform precision tests of fundamental principles, such as the equivalence principle (*37*, *43*, *44*, *59*).

REFERENCES AND NOTES

1. M. H. Anderson, J. R. Ensher, M. R. Matthews, C. E. Wieman, E. A. Cornell, Observation of Bose-Einstein condensation in a dilute atomic vapor. *Science* **269**, 198–201 (1995). doi: 10.1126/science.269.5221.198; pmid: 17789847
2. K. B. Davis, M. Mewes, M. R. Andrews, N. J. van Druten, D. S. Durfee, D. M. Kurn, W. Ketterle, Bose-Einstein condensation in a gas of sodium atoms. *Phys. Rev. Lett.* **75**, 3969–3973 (1995). doi: 10.1103/PhysRevLett.75.3969; pmid: 10059782
3. B. DeMarco, D. S. Jin, Onset of fermi degeneracy in a trapped atomic gas. *Science* **285**, 1703–1706 (1999). doi: 10.1126/science.285.5434.1703; pmid: 10481000
4. I. Bloch, J. Dalibard, S. Nascimbène, Quantum simulations with ultracold quantum gases. *Nat. Phys.* **8**, 267–276 (2012). doi: 10.1038/nphys2259
5. I. Bloch, J. Dalibard, W. Zwerger, Many-body physics with ultracold gases. *Rev. Mod. Phys.* **80**, 885–964 (2008). doi: 10.1103/RevModPhys.80.885
6. C. Gross, I. Bloch, Quantum simulations with ultracold atoms in optical lattices. *Science* **357**, 995–1001 (2017). doi: 10.1126/science.aal3837; pmid: 28883070
7. A. D. Cronin, J. Schmiedmayer, D. E. Pritchard, Optics and interferometry with atoms and molecules. *Rev. Mod. Phys.* **81**, 1051–1129 (2009). doi: 10.1103/RevModPhys.81.1051
8. C. L. Degen, F. Reinhard, P. Cappellaro, Quantum sensing. *Rev. Mod. Phys.* **89**, 035002 (2017). doi: 10.1103/RevModPhys.89.035002
9. S. L. Campbell, R. B. Hutson, G. E. Marti, A. Goban, N. Darkwah Oppong, R. L. McNally, L. Sonderhouse, J. M. Robinson, W. Zhang, B. J. Bloom, J. Ye, A Fermi-degenerate three-dimensional optical lattice clock. *Science* **358**, 90–94 (2017). doi: 10.1126/science.aam5538; pmid: 28983047
10. M. Greiner, O. Mandel, T. Esslinger, T. W. Hänsch, I. Bloch, Quantum phase transition from a superfluid to a Mott insulator in a gas of ultracold atoms. *Nature* **415**, 39–44 (2002). doi: 10.1038/415039a; pmid: 11780110
11. T. Giamarchi, H. J. Schulz, Anderson localization and interactions in one-dimensional metals. *Phys. Rev. B* **37**, 325–340 (1988). doi: 10.1103/physrevb.37.325; pmid: 9943580

Downloaded from https://www.science.org at Peking University on November 05, 2026

12. H. Yao, T. Giamarchi, L. Sanchez-Palencia, Lieb-Liniger Bosons in a shallow quasiperiodic potential: Bose glass phase and fractal mott lobes. *Phys. Rev. Lett.* **125**, 060401 (2020). doi: 10.1103/PhysRevLett.125.060401; pmid: 32845659
13. D. N. Aguilera, H. Ahlers, B. Battelier, A. Bawamia, A. Bertoldi, R. Bondarescu, K. Bongs, P. Bouyer, C. Braxmaier, L. Cacciapuoti, C. Chaloner, M. Chwalla, W. Ertmer, M. Franz, N. Gaaloul, M. Gehler, D. Gerardi, L. Gesa, N. Gürlebeck, J. Hartwig, M. Hauth, O. Hellmig, W. Herr, S. Herrmann, A. Heske, A. Hinton, P. Ireland, P. Jetzer, U. Johann, M. Krutzik, A. Kubelka, C. Lämmerzahl, A. Landragin, I. Lloro, D. Massonnet, I. Mateos, A. Milke, M. Nofrarias, M. Oswald, A. Peters, K. Posso-Trujillo, E. Rasel, E. Rocco, A. Roura, J. Rudolph, W. Schleich, C. Schubert, T. Schuldt, S. Seidel, K. Sengstock, C. F. Sopuerta, F. Sorrentino, D. Summers, G. M. Tino, C. Trenkel, N. Uzunoglu, W. von Klitzing, R. Walser, T. Wendrich, A. Wenzlawski, P. Weßels, A. Wicht, E. Wille, M. Williams, P. Windpassinger, N. Zahzam, STE-QUEST—test of the universality of free fall using cold atom interferometry. *Class. Quantum Grav.* **31**, 115010 (2014). doi: 10.1088/0264-9381/31/11/115010
14. S. Dimopoulos, P. W. Graham, J. M. Hogan, M. A. Kasevich, Testing general relativity with atom interferometry. *Phys. Rev. Lett.* **98**, 111102 (2007). doi: 10.1103/PhysRevLett.98.111102; pmid: 17501039
15. P. W. Graham, J. M. Hogan, M. A. Kasevich, S. Rajendran, New method for gravitational wave detection with atomic sensors. *Phys. Rev. Lett.* **110**, 171102 (2013). doi: 10.1103/PhysRevLett.110.171102; pmid: 23679702
16. S. Dimopoulos, P. W. Graham, J. M. Hogan, M. A. Kasevich, S. Rajendran, Gravitational wave detection with atom interferometry. *Phys. Lett. B* **678**, 37–40 (2009). doi: 10.1016/j.physletb.2009.06.011
17. B. Elder, J. Khoury, P. Haslinger, M. Jaffe, H. Müller, P. Hamilton, Chameleon dark energy and atom interferometry. *Phys. Rev. D* **94**, 044051 (2016). doi: 10.1103/PhysRevD.94.044051
18. A. E. Leanhardt, T. A. Pasquini, M. Saba, A. Schirotzek, Y. Shin, D. Kielpinski, D. E. Pritchard, W. Ketterle, Cooling Bose-Einstein condensates below 500 picokelvin. *Science* **301**, 1513–1515 (2003). doi: 10.1126/science.108882; pmid: 12970559
19. P. Medley, D. M. Weld, H. Miyake, D. E. Pritchard, W. Ketterle, Spin gradient demagnetization cooling of ultracold atoms. *Phys. Rev. Lett.* **106**, 195301 (2011). doi: 10.1103/PhysRevLett.106.195301; pmid: 21668171
20. T. Kovachy, J. M. Hogan, A. Sugarbaker, S. M. Dickerson, C. A. Donnelly, C. Overstreet, M. A. Kasevich, Matter wave lensing to picokelvin temperatures. *Phys. Rev. Lett.* **114**, 143004 (2015). doi: 10.1103/PhysRevLett.114.143004; pmid: 25910118
21. X. Chen, B. Fan, The emergence of picokelvin physics. *Rep. Prog. Phys.* **83**, 076401 (2020). doi: 10.1088/1361-6633/ab8ab6; pmid: 32303019
22. O. J. Luiten, M. W. Reynolds, J. T. M. Walraven, Kinetic theory of the evaporative cooling of a trapped gas. *Phys. Rev. A* **53**, 381–389 (1996). doi: 10.1103/physreva.53.381; pmid: 9912894
23. C. A. Sackett, Limits on weak magnetic confinement of neutral atoms. *Phys. Rev. A* **73**, 013626 (2006). doi: 10.1103/PhysRevA.73.013626
24. T. van Zoest, N. Gaaloul, Y. Singh, H. Ahlers, W. Herr, S. T. Seidel, W. Ertmer, E. Rasel, M. Eckart, E. Kajari, S. Arnold, G. Nandi, W. P. Schleich, R. Walser, A. Vogel, K. Sengstock, K. Bongs, W. Lewoczko-Adamczyk, M. Schiemangk, T. Schuldt, A. Peters, T. Könemann, H. Müntinga, C. Lämmerzahl, H. Dittus, T. Steinmetz, T. W. Hänsch, J. Reichel, Bose-Einstein condensation in microgravity. *Science* **328**, 1540–1543 (2010). doi: 10.1126/science.1189164; pmid: 20558713
25. H. Müntinga, H. Ahlers, M. Krutzik, A. Wenzlawski, S. Arnold, D. Becker, K. Bongs, H. Dittus, H. Duncker, N. Gaaloul, C. Gherasim, E. Giese, C. Grzeschik, T. W. Hänsch, O. Hellmig, W. Herr, S. Herrmann, E. Kajari, S. Kleinert, C. Lämmerzahl, W. Lewoczko-Adamczyk, J. Malcolm, N. Meyer, R. Nolte, A. Peters, M. Popp, J. Reichel, A. Roura, J. Rudolph, M. Schiemangk, M. Schneider, S. T. Seidel, K. Sengstock, V. Tamma, T. Valenzuela, A. Vogel, R. Walser, T. Wendrich, P. Windpassinger, W. Zeller, T. van Zoest, W. Ertmer, W. P. Schleich, E. M. Rasel, Interferometry with Bose-Einstein condensates in microgravity. *Phys. Rev. Lett.* **110**, 093602 (2013). doi: 10.1103/PhysRevLett.110.093602; pmid: 23496709
26. C. Deppner, W. Herr, M. Cornelius, P. Stromberger, T. Sternke, C. Grzeschik, A. Grote, J. Rudolph, S. Herrmann, M. Krutzik, A. Wenzlawski, R. Corgier, E. Charron, D. Guéry-Odelin, N. Gaaloul, C. Lämmerzahl, A. Peters, P. Windpassinger, E. M. Rasel, Collective-mode enhanced matter-wave optics. *Phys. Rev. Lett.* **127**, 100401 (2021). doi: 10.1103/PhysRevLett.127.100401; pmid: 34533345
27. G. Condon, M. Rabault, B. Barrett, L. Chichet, R. Arguel, H. Eneriz-Imaz, D. Naik, A. Bertoldi, B. Battelier, P. Bouyer, A. Landragin, All-optical Bose-Einstein condensates in microgravity. *Phys. Rev. Lett.* **123**, 240402 (2019). doi: 10.1103/PhysRevLett.123.240402; pmid: 31922832
28. G. Stern, B. Battelier, R. Geiger, G. Varoquaux, A. Villing, F. Moron, O. Carraz, N. Zahzam, Y. Bidel, W. Chaibi, F. Pereira dos Santos, A. Bresson, A. Landragin, P. Bouyer, Light-pulse atom interferometry in microgravity. *Eur. Phys. J. D* **53**, 353–357 (2009). doi: 10.1140/epjd/e2009-00150-5
29. R. Geiger, V. Ménoret, G. Stern, N. Zahzam, P. Cheinet, B. Battelier, A. Villing, F. Moron, M. Lours, Y. Bidel, A. Bresson, A. Landragin, P. Bouyer, Detecting inertial effects with airborne matter-wave interferometry. *Nat. Commun.* **2**, 474 (2011). doi: 10.1038/ncomms1479; pmid: 21934658
30. B. Barrett, L. Antoni-Micollier, L. Chichet, B. Battelier, T. Lévèque, A. Landragin, P. Bouyer, Dual matter-wave inertial sensors in weightlessness. *Nat. Commun.* **7**, 13786 (2016). doi: 10.1038/ncomms13786; pmid: 27941928
31. D. Becker, M. D. Lachmann, S. T. Seidel, H. Ahlers, A. N. Dinkelaker, J. Grosse, O. Hellmig, H. Müntinga, V. Schkolnik, T. Wendrich, A. Wenzlawski, B. Weps, R. Corgier, T. Franz, N. Gaaloul, W. Herr, D. Lüdtke, M. Popp, S. Amri, H. Duncker, M. Erbe, A. Kohfeldt, A. Kubelka-Lange, C. Braxmaier, E. Charron, W. Ertmer, M. Krutzik, C. Lämmerzahl, A. Peters, W. P. Schleich, K. Sengstock, R. Walser, A. Wicht, P. Windpassinger, E. M. Rasel, Space-borne Bose–Einstein condensation for precision interferometry. *Nature* **562**, 391–395 (2018). doi: 10.1038/s41586-018-0605-1; pmid: 30333576
32. N. Gaaloul, M. Meister, R. Corgier, A. Pichery, P. Boegel, W. Herr, H. Ahlers, E. Charron, J. R. Williams, R. J. Thompson, W. P. Schleich, E. M. Rasel, N. P. Bigelow, A space-based quantum gas laboratory at picokelvin energy scales. *Nat. Commun.* **13**, 7889 (2022). doi: 10.1038/s41467-022-35274-6; pmid: 6550117
33. M. S. Safronova, D. Budker, D. DeMille, D. F. J. Kimball, A. Derevianko, C. W. Clark, Search for new physics with atoms and molecules. *Rev. Mod. Phys.* **90**, 025008 (2018). doi: 10.1103/RevModPhys.90.025008
34. D. C. Aveline, J. R. Williams, E. R. Elliott, C. Dutenhoffer, J. R. Kellogg, J. M. Kohel, N. E. Lay, K. Oudrhiri, R. F. Shotwell, N. Yu, R. J. Thompson, Observation of Bose-Einstein condensates in an Earth-orbiting research lab. *Nature* **582**, 193–197 (2020). doi: 10.1038/s41586-020-2346-1; pmid: 32528092
35. K. Frye, S. Abend, W. Bartosch, A. Bawamia, D. Becker, H. Blume, C. Braxmaier, S. W. Chiow, M. A. Efremov, W. Ertmer, P. Fierlinger, T. Franz, N. Gaaloul, J. Grosse, C. Grzeschik, O. Hellmig, V. A. Henderson, W. Herr, U. Israelsson, J. Kohel, M. Krutzik, C. Kürbis, C. Lämmerzahl, M. List, D. Lüdtke, N. Lundblad, J. P. Marburger, M. Meister, M. Mihm, H. Müller, H. Müntinga, A. M. Nepal, T. Oberschulte, A. Papakonstantinou, J. Perovšek, A. Peters, A. Prat, E. M. Rasel, A. Roura, M. Sbroscia, W. P. Schleich, C. Schubert, S. T. Seidel, J. Sommer, C. Spindeldreier, D. Stamper-Kurn, B. K. Stuhl, M. Warner, T. Wendrich, A. Wenzlawski, A. Wicht, P. Windpassinger, N. Yu, L. Wörner, The Bose-Einstein condensate and cold atom laboratory. *EPJ Quantum Technol.* **8**, 1 (2021). doi: 10.1140/epjqt/s40507-020-00090-8
36. R. A. Carollo, D. C. Aveline, B. Rhyno, S. Vishveshwara, C. Lannert, J. D. Murphree, E. R. Elliott, J. R. Williams, R. J. Thompson, N. Lundblad, Observation of ultracold atomic bubbles in orbital microgravity. *Nature* **606**, 281–286 (2022). doi: 10.1038/s41586-022-04639-8; pmid: 35585238
37. E. R. Elliott, D. C. Aveline, N. P. Bigelow, P. Boegel, S. Botsi, E. Charron, J. P. D'Incao, P. Engels, T. Estrampes, N. Gaaloul, J. R. Kellogg, J. M. Kohel, N. E. Lay, N. Lundblad, M. Meister, M. E. Mossman, G. Müller, H. Müller, K. Oudrhiri, L. E. Phillips, A. Pichery, E. M. Rasel, C. A. Sackett, M. Sbroscia, W. P. Schleich, R. J. Thompson, J. R. Williams, Quantum gas mixtures and dual-species atom interferometry in space. *Nature* **623**, 502–508 (2023). doi: 10.1038/s41586-023-06645-w; pmid: 37968524
38. D. M. Stamper-Kurn, M. Ueda, Spinor Bose gases: Symmetries, magnetism, and quantum dynamics. *Rev. Mod. Phys.* **85**, 1191–1244 (2013). doi: 10.1103/RevModPhys.85.1191
39. C. Vogt, M. Woltmann, S. Herrmann, C. Lämmerzahl, H. Albers, D. Schlippert, E. M. Rasel, PRIMUS, Evaporative cooling from an optical dipole trap in microgravity. *Phys. Rev. A* **101**, 013634 (2020). doi: 10.1103/PhysRevA.101.013634
40. L. Wang, P. Zhang, X.-Z. Chen, Z.-Y. Ma, Generating a picokelvin ultracold atomic ensemble in microgravity. *J. Phys. B. At. Mol. Opt. Phys.* **46**, 195302 (2013). doi: 10.1088/0953-4075/46/19/195302
41. H. Yao, T. Luan, C. Li, Y. Zhang, Z. Ma, X. Chen, Comparison of different techniques in optical trap for generating picokelvin 3D atom cloud in microgravity. *Opt. Commun.* **359**, 123–128 (2016). doi: 10.1016/j.optcom.2015.09.065
42. H. Li, J. Yu, X. Yuan, B. Wu, Y. Xie, L. Li, A. Liang, M. Huang, S. Jin, W. Xiong, B. Wang, D. Chen, T. Li, X. Hou, L. Liu, X. Zhou, W. Chen, X. Chen, Deep cooling scheme of quantum degenerate gas and ground experimental verification for chinese space station. *Front. Phys.* **10**, 971059 (2022). doi: 10.3389/fphy.2022.971059
43. J. Williams, S.-w. Chiow, N. Yu, H. Müller, Quantum test of the equivalence principle and space-time aboard the International Space Station. *New J. Phys.* **18**, 025018 (2016). doi: 10.1088/1367-2630/18/2/025018
44. C. Overstreet, P. Asenbaum, T. Kovachy, R. Notermans, J. M. Hogan, M. A. Kasevich, Effective inertial frame in an atom interferometric test of the equivalence principle. *Phys. Rev. Lett.* **120**, 183604 (2018). doi: 10.1103/PhysRevLett.120.183604; pmid: 29775337
45. M. D. Lachmann, H. Ahlers, D. Becker, A. N. Dinkelaker, J. Grosse, O. Hellmig, H. Müntinga, V. Schkolnik, S. T. Seidel, T. Wendrich, A. Wenzlawski, B. Carrick, N. Gaaloul, D. Lüdtke, C. Braxmaier, W. Ertmer, M. Krutzik, C. Lämmerzahl, A. Peters, W. P. Schleich, K. Sengstock, A. Wicht, P. Windpassinger, E. M. Rasel, Ultracold atom interferometry in space. *Nat. Commun.* **12**, 1317 (2021). doi: 10.1038/s41467-021-21628-z; pmid: 33637769

Downloaded from https://www.science.org at Peking University on November 05, 2026

46. J. R. Williams, C. A. Sackett, H. Ahlers, D. C. Aveline, P. Boegel, S. Botsi, E. Charron, E. R. Elliott, N. Gaaloul, E. Giese, W. Herr, J. R. Kellogg, J. M. Kohel, N. E. Lay, M. Meister, G. Müller, H. Müller, K. Oudrhiri, L. Phillips, A. Pichery, E. M. Rasel, A. Roura, M. Sbroscia, W. P. Schleich, C. Schneider, C. Schubert, B. Sen, R. J. Thompson, N. P. Bigelow, Pathfinder experiments with atom interferometry in the Cold Atom Lab onboard the International Space Station. *Nat. Commun.* **15**, 6414 (2024). doi: 10.1038/s41467-024-50585-6; pmid: 39138156
47. L. Li, C. Zhou, W. Xiong, M. Huang, S. Fang, X. Xu, J. Ji, M. Gao, T. Song, Y. Hong, Z. Liang, D. Chen, X. Hou, X. Zhou, X. Chen, W. Chen, B. Wang, T. Li, L. Liu, All-fiber laser system for all-optical ^{87}Rb Bose Einstein condensate to space application. *Appl. Optics* **62**, 7844–7851 (2023). doi: 10.1364/AO.497749; pmid: 37855495
48. L. Li, W. Xiong, B. Wang, T. Li, Y. Xie, A. Liang, The design, realization, and validation of the scheme for quantum degenerate research in microgravity. *IEEE Photon. J.* **15**, 1–8 (2023). doi: 10.1109/JPHOT.2023.3266108
49. See supplementary materials.
50. D. M. Stamper-Kurn, M. R. Andrews, A. P. Chikkatur, S. Inouye, H. J. Miesner, J. Stenger, W. Ketterle, Optical confinement of a bose-einstein condensate. *Phys. Rev. Lett.* **80**, 2027–2030 (1998). doi: 10.1103/PhysRevLett.80.2027
51. C.-L. Hung, X. Zhang, N. Gemelke, C. Chin, Accelerating evaporative cooling of atoms into Bose-Einstein condensation in optical traps. *Phys. Rev. A* **78**, 011604 (2008). doi: 10.1103/PhysRevA.78.011604
52. A. G. Truscott, K. E. Strecker, W. I. McAlexander, G. B. Partridge, R. G. Hulet, Observation of fermi pressure in a gas of trapped atoms. *Science* **291**, 2570–2572 (2001). doi: 10.1126/science.1059318; pmid: 11283362
53. Y. Fan, S. Shi, L. Cao, Q. Zhang, D. Hu, Y. Wang, X. Zhou, Spin polarization control via magnetic field in dissipative bosonic systems. *Front. Phys.* **21**, 12200 (2026).
54. M.-S. Chang, C. D. Hamley, M. D. Barrett, J. A. Sauer, K. M. Fortier, W. Zhang, L. You, M. S. Chapman, Observation of spinor dynamics in optically trapped ^{87}RB bose-einstein condensates. *Phys. Rev. Lett.* **92**, 140403 (2004). doi: 10.1103/PhysRevLett.92.140403; pmid: 15089521
55. J. S. Haase, A. Fieguth, I. Bröckel, J. Hamann, J. Kruse, C. Klempt, Robust and compact single-lens crossed-beam optical dipole trap for Bose-Einstein condensation in microgravity. *EPJ Quantum Technol.* **12**, 116 (2025). doi: 10.1140/epjqt/s40507-025-00421-7
56. F. D. M. Haldane, 'Luttinger liquid theory' of one-dimensional quantum fluids. I. Properties of the Luttinger model and their extension to the general 1D interacting spinless Fermi gas. *J. Phys. C. Solid State Phys.* **14**, 2585–2609 (1981). doi: 10.1088/0022-3719/14/19/010
57. T. Giamarchi, *Quantum Physics in One Dimension* (Carendon Press, Oxford, 2003).
58. M. A. Cazalilla, R. Citro, T. Giamarchi, E. Orignac, M. Rigol, One dimensional bosons: From condensed matter systems to ultracold gases. *Rev. Mod. Phys.* **83**, 1405–1466 (2011). doi: 10.1103/RevModPhys.83.1405
59. P. Asenbaum, C. Overstreet, M. Kim, J. Curti, M. A. Kasevich, Atom-interferometric test of the equivalence principle at the 10^{-12} level. *Phys. Rev. Lett.* **125**, 191101 (2020). doi: 10.1103/PhysRevLett.125.191101; pmid: 33216577
60. Data set is available from Zenodo at 10.5281/zenodo.18217600.
61. R. Grimm, M. Weidemüller, Y. B. Ovchinnikov, Optical dipole traps for neutral atoms, in *Advances in Atomic, Molecular, and Optics Physics*, B. Bederson, H. Walther, eds. (Academic Press, 2000), vol. 42, pp. 95–170.

ACKNOWLEDGMENTS

We thank Yidong Gu, Dajun Wang, Xiong-Jun Liu, Tianwei Zhou, Yaoyuan Fan, Wenlan Chen, Shuai Chen, Bing Yang, Bo Yan, Jing Zhang, Rong-Gen Cai, Guoning Liu, and Su Yi for helpful discussions. **Funding:** This work was supported by the National Key Research and Development Program of China (grants 2021YFA0718300 and 2021YFA1400900), the Space Application System of China Manned Space Program, and the National Natural Science Foundation of China (grant 92365208). **Author contributions:** W. X., T. L., and S. J. designed, constructed, and operated the CAPR system aboard the space station, optimized the experimental timing sequences, and performed data collection and analysis. Q. H., L. L., C.-K. L., Z. Z., X. L., and Y. G. contributed to optimizing the in-orbit experimental sequences and analyzing the data. Y. H., X. Z., W. C., and X. C. coordinated the CAPR experiments with the operation of the space station systems. W. X., T. L., S. J., Y. H., B. W., L. L., D. C., T. S., J. J., C. Z., J. T., X. H., L. L., X. Z., W. C., and X. C. participated in the system design and construction. C.-K. L., Z. Z., X. L., Y. G., and H. Y. performed numerical simulations and theoretical analysis. X. Z., W. C., and X. C. jointly supervised the project. All authors read, edited, and approved the final manuscript. **Competing interests:** There are no competing interests to declare. **Data, code, and materials availability:** The data shown in this manuscript is available via Zenodo (*60*). No new materials were generated for this study. **License information:** Copyright © 2026 the authors, some rights reserved; exclusive licensee American Association for the Advancement of Science. No claim to original US government works. https://www.science.org/about/science-licenses-journal-article-reuse

SUPPLEMENTARY MATERIALS

science.org/doi/10.1126/science.aea5324
Materials and Methods; Supplementary Text; Figs. S1 to S3; Reference (*61*)

Submitted 12 July 2025; accepted 22 October 2026; published online 5 November 2026
10.1126/science.aea5324

Downloaded from https://www.science.org at Peking University on November 05, 2026

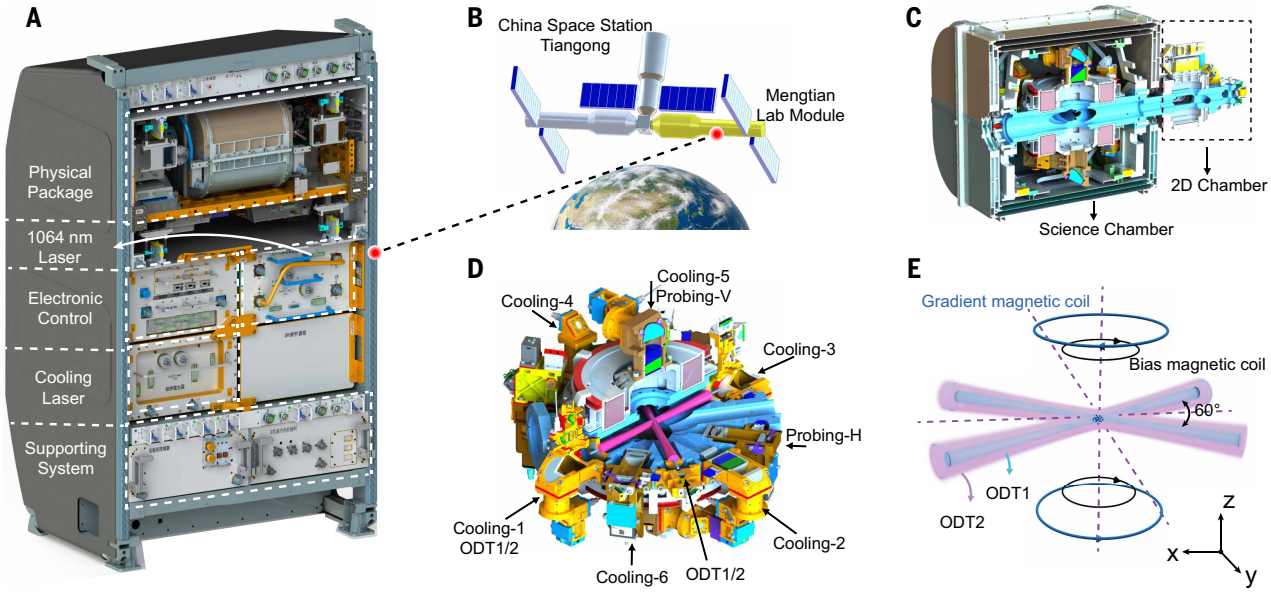


Fig. 1. The Cold Atom Physics Rack (CAPR) hardware configuration. (**A**) Overall modular architecture: the system comprises five components (top to bottom): physical package, 1064 nm laser module, the electronic control module, cooling laser module, supporting system handling power/water supply. (**B**) CAPR is housed within the Mengtian Laboratory Module of the China Space Station, *Tiangong*. (**C**) The inside view of the physical package: contains dual interconnected vacuum chambers. The 2D magneto-optical trap (MOT) chamber (2D Chamber) interfaces with a rubidium atomic source and an 8 L/s ion pump at one end, while connecting via a differential tube to the Science Chamber maintained by a 75 L/s ion pump and getter pump, with a vacuum level below 5×10^{-9} Pa. Thermally activated rubidium vapor flows into the 2D Chamber for preliminary cooling, after which atoms are transferred to the Science Chamber for 3D MOT recapture. (**D**) Science Chamber integrates six cooling optical paths Cooling-1 to 6, two crossed optical dipole traps (ODT1: blue, 54 m beam waist radius; ODT2: purple, 124 m beam waist radius) and orthogonal detection systems (Probing-H and Probing-V). Both ODTs employ 1064 nm lasers, with ODT1 enabling tight confinement and ODT2 providing extended trapping volumes. (**E**) Experimental setup for two-stage cooling, including two pairs of crossed ODTs and magnetic field coils. The two beams of each ODT intersect at 60°. The magnetic coil system consists of a Helmholtz pair (Bias magnetic coil) generating a bias magnetic field and an anti-Helmholtz pair (Gradient magnetic coil) producing a quadrupole magnetic trap and magnetic field gradient. The *x*, *y*, *z* coordinates are illustrated, where the *x*- and *y*-axes correspond to the angular bisectors of the intersecting ODT beams. Probing-H and Probing-V detection beams propagate along the *y*- and *z*-axes, respectively.

Downloaded from https://www.science.org at Peking University on November 05, 2026

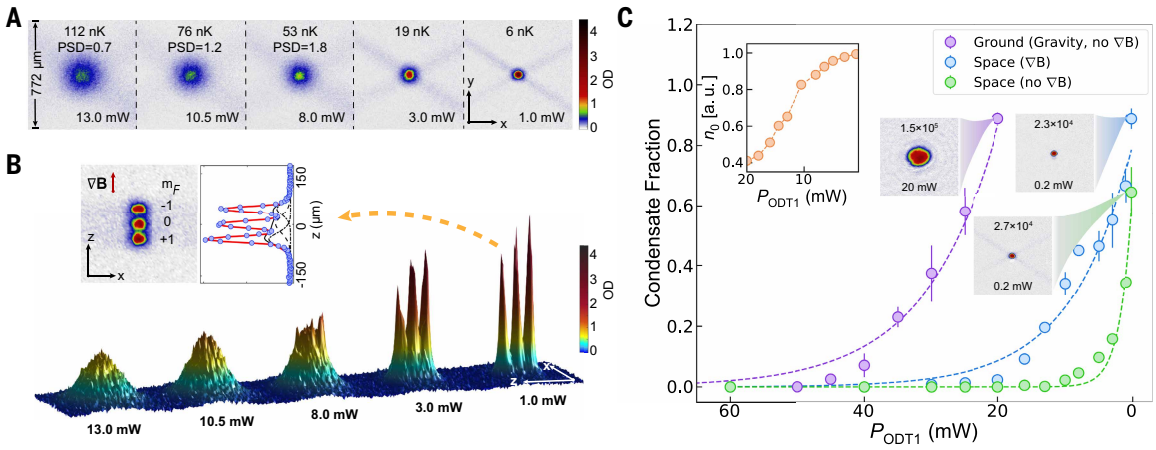


Fig. 2. BEC formation via ODT evaporation in space. (**A**) Absorption images (on the *xy*-plane) of the atoms under evaporation cooling at different ODT1 shutdown powers P_{ODT1}. As P_{ODT1} decreases from 13.0 mW to 1.0 mW, the atomic temperature drops from 112 nK to 6 nK. The phase-space density (PSD) increases from 0.7 to 1.8 as P_{ODT1} decreases from 13.0 mW to 8.0 mW. Absorption images of atoms are obtained after 30 ms time-of-flight (TOF) expansion. OD indicates optical density. (**B**) Absorption images showing the spatial distributions of three separated spin components at different P_{ODT1} following the Stern–Gerlach sequence. Inset: Atomic distribution in the *xz*-plane following Stern-Gerlach separation at $P_{ODT1} = 1.0$ mW. The left panel is absorption image with magnetic field gradient ∇B aligned along the *z*-axis. The right panel is density profile along *z*-axis (blue circles) fitted to three bimodal distributions (red solid lines) corresponding to three Zeeman states $|F = 1, m_F = +1, 0, -1\rangle$. Black dash-dotted curves denote thermal components of individual Zeeman states; solid black curve represents the total thermal population. (**C**) Condensate fraction versus P_{ODT1} for ground (purple), space without (green) and with (blue) magnetic field gradient ∇B. Dashed lines indicate exponential fits illustrating trend evolution. The data points and error bars represent the mean and standard deviation of three measurements. Left inset: Relative population of atoms in the $|F = 1, m_F = 0\rangle$ state, denoted as n_0, versus P_{ODT1}. Right insets: Absorption images comparing experiments on the ground (20 ms TOF, $P_{ODT1} = 20$ mW), and in space both with and without ∇B (30 ms TOF, $P_{ODT1} = 0.2$ mW).

Downloaded from https://www.science.org at Peking University on November 05, 2026

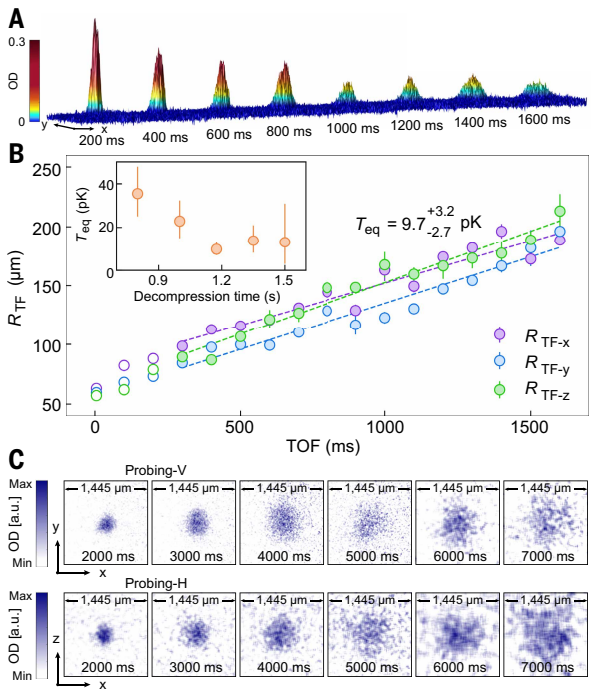


Fig. 3. Evaluation of ultracold atomic equivalent temperature in space. (**A**) Single-shot absorption images of the atomic cloud in the *xy*-plane at short TOFs (200 ms to 1600 ms), with approximately 2×10^4 atoms. (**B**) Equivalent temperature measurements and evaluation. The purple, blue and green circles correspond to atomic cloud sizes, i.e., the Thomas–Fermi radii R_{TF-i} ($i = x, y, z$), versus TOFs along the x, y, and z directions, respectively. The atomic cloud sizes along x- and y-axis are obtained from the Probing-V images, and the z-axis size is extracted from the Probing-H images. The equivalent temperature is evaluated from the expansion of the atomic cloud by a linear fit to the TOF data between 300 and 1600 ms. The equivalent temperature reaches as low as $T_{eq} = 9.7^{+3.2}_{-2.7}$ pK after quasi-adiabatic decompression in ODT2. Inset panel: The equivalent temperature measured at different decompression times. (**C**) Single-shot images of atomic cloud at longer TOFs (2000 ms to 7000 ms). The upper row shows the cloud in the *xy*-plane (from Probing-V), and the lower row shows the *xy*-plane (from Probing-H).

Downloaded from https://www.science.org at Peking University on November 05, 2026

Science
AAAS

Quantum gases below 10 picokelvin in space

Wei Xiong, Tang Li, Shengjie Jin, Qi Huang, Bin Wang, Lin Li, Yufeng He, Xiaopeng Li, Dijun Chen, Tieqiang Song, Jingwei Ji, Cuiyun Zhou, Chi-Kin Lai, Zhengxi Zhang, Jinyuan Tian, Yajing Guo, Hepeng Yao, Xia Hou, Liang Liu, Xiaoji Zhou, Weibiao Chen, and Xuzong Chen

*Science***Ahead of Print** DOI: 10.1126/science.aea5324

View the article online
https://www.science.org/doi/10.1126/science.aea5324
Permissions
https://www.science.org/help/reprints-and-permissions

Downloaded from https://www.science.org at Peking University on November 05, 2026

Use of this article is subject to the Terms of service

Science (ISSN 1095-9203) is published by the American Association for the Advancement of Science. 1200 New York Avenue NW, Washington, DC 20005. The title *Science* is a registered trademark of AAAS.

Copyright © 2026 The Authors, some rights reserved; exclusive licensee American Association for the Advancement of Science. No claim to original U.S. Government Works